Electronic Supplementary Information:

Anisotropic Lattice Softening Near the Structural Phase Transition in the Thermosalient Crystal 1,2,4,5-tetrabromobenzene

Boris A. Zakharov,[ab]† Adam A.L. Michalchuk,[bcd] Carole A. Morrison[c] and Elena V. Boldyreva[ab]

1. X-RAY DIFFRACTION EXPERIMENTS WITH MULTIPLE CRYSTALS

A remarkable feature of the thermosalient effect in 1,2,4,5-tetrabromobenzene was observed for a crystals mounted with oil onto a micro-mesh sample holder. This is that the mechanical response (crystal disappearing from holder) and the structural phase transition (the change in the crystal structure) were well separated in time at a fixed temperature, or in temperature on continuous heating. The phase transition clearly preceded crystal jumping from the holder, and loss of the crystal from the holder was not observed at the moment of the phase transition. Similar behaviour was observed for ferrocene: the crystal disintegration and the phase transition on cooling were shown to be two separate phenomena. For ferrocene, disintegration could not be repeated even after powder had been heated to ambient temperature (J. S. Bodenheimer and W. Low, *Phys. Lett. A*, 1971, **36**, 253–254). A crystal "locked" in a capillary with oil for a diffraction experiment cannot jump. A crystal in a holder does jump, but it is only very rarely that after this jump at least a part of the crystal still remains on the holder, accessible for structure determination. The changes in lattice parameters of all tested crystals of 1,2,4,5-tetrabromobenzene *vs*. temperature are plotted in Figure S1. In our experiments crystal disappearing from crystal holder occurred only for one crystal. Apart from that presented in the main text, another possible explanation of crystal disappearing from a *MiTiGen* holder during a single-crystal X-ray diffraction experiment after the phase transition has been observed is sublimation. We cannot exclude this option completely, since we did not see the moments when the crystals disappeared. However, we note that this explanation is unlikely. No notable and consistent decay in the reflection intensities was observed at a fixed temperature, before a crystal disappeared. Besides, it seems unlikely that a crystal would completely disappear because of sublimation at 313 K when covered by oil, but not even at 343 K when placed inside an open capillary.

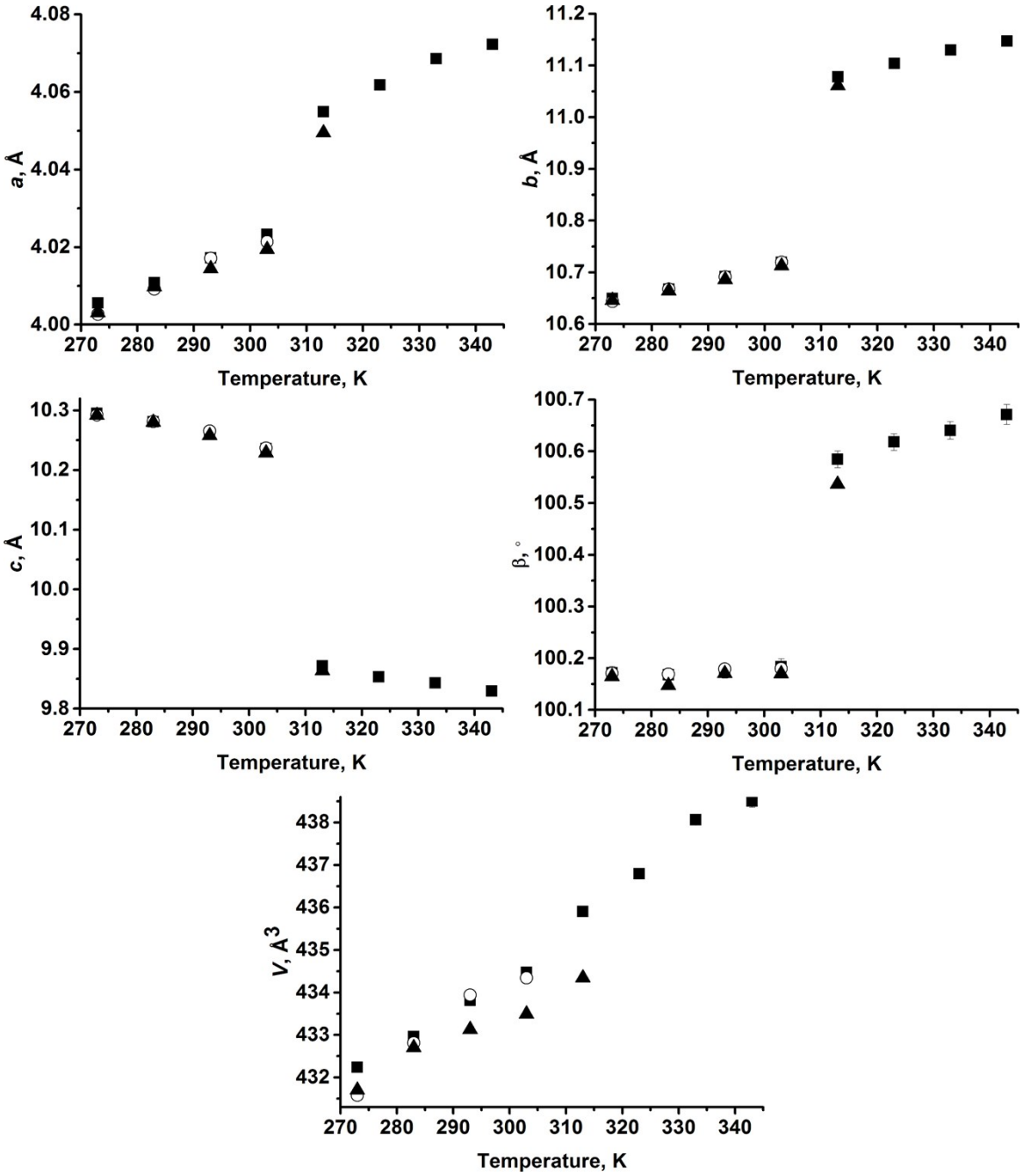

Figure S1. Dependence of the 1,2,4,5-tetrabromobenzene lattice parameters on temperature (experiment with crystal fixed in capillary – squares, experiment with crystals fixed at micro-mesh sample holder – circles and triangles, respectively)

2. CONVERGENCE TESTING FOR DFT CALCULATIONS

To ensure accuracy of the theoretical model, it is imperative to ensure sufficient sampling of the Brillouin zone is used. To test convergence of *k*-space, single point energy calculations were performed using a cut-off energy of 900 eV with norm-conserving pseudopotentials, Figure S2. It has been previously suggested that a spacing of 0.08 $Å^{-1}$ is generally acceptable for structural optimisation (J. Binns, M. R. Healy, S. Parsons and C. A. Morrison, *Acta Cryst. B.*, 2014, **70**, 259–267.) as is seen here with a ΔE/ion of < 1meV at this spacing. However, to ensure accurate phonon calculations, notably tighter convergence is required. For convergence testing of the kinetic energy cut-off, the converged *k*-point grid (522) was used, Figure S2.

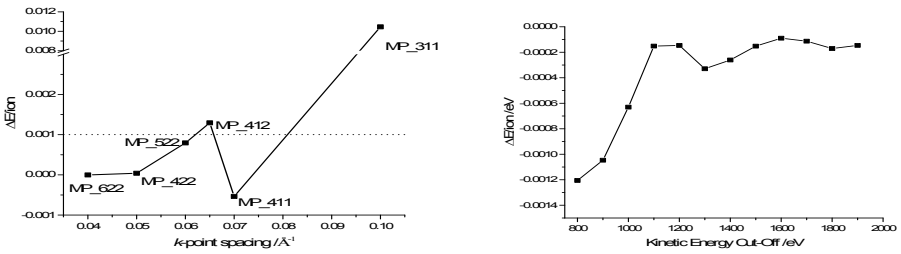

Figure S2: Convergence testing for DFT calculations of TBB. (Left) convergence of *k*-point sampling grid, with MP grids labelled, and (Right) convergence of kinetic energy cut-off.

3. SYMMETRY ADAPTED PERTURBATION THEORY CALCULATIONS

Within symmetry adapted perturbation theory (SAPT), the total interaction energy can be written as

$$E_{IE}^{SAPT} = \sum_{n=1}^{\infty}\sum_{k=0}^{\infty}\sum_{l=0}^{\infty}(E_{pol}^{(nkl)} + E_{exch}^{(nkl)})$$

Here, the total interaction energy (E_{IE}) is given by expansion of the polarisation term (typically attractive), E_{pol}, and the exchange term (typically repulsive), E_{exch}. The latter is due to the antisymmetrization of the wavefunction. These terms are expanded across the order of intermolecular potential, *n*, and intramonomer electron correlation, *k* and *l*. The SAPT0 method treats each interacting monomer within the Hartree-Fock level and adds explicit dispersion terms, which result from second order perturbation theory. This is added to the electrostatic, exchange and induction terms. SAPT0 can therefore be thought of as largely analogous to an MP2-type calculation, with interaction energy for SAPT0 given as,

$$E_{IE}^{SAPT0} = E_{IE}^{HF} + \left[E_{disp}^{(20)} + E_{exch-disp}^{(20)}\right]_{disp}$$

$$= [E_{elst}^{(10)}]_{elst} + [E_{exch}^{(10)}]_{exch} + [E_{ind,r}^{(20)} + E_{exch-ind,r}^{(20)} + \delta E_{HF}^{(2)}]_{ind} + [E_{disp}^{(20)} + E_{exch-disp}^{(20)}]_{disp}$$

Thus, the energy is broken into traditional electrostatic (E_{elst}), exchange (E_{exch}), inductive (E_{ind}) and dispersion (E_{disp}) interaction energies. In the above, $E^{(v,w)}$ represent the interaction energy at perturbation level *v*=*n*, with *w*=*k*+*l*. A complete description can be found elsewhere (Parker *et al* JCP, 140, 2014). Within the sSAPT method, employed here, the exchange term is scaled based on empirically-fitted scaling coefficients (Lao and Herbert, JPC A 116, 3042, 2012), and has been shown to provide excellent results for calculated energies (Parker *et al* JCP 140, 2014).

In the present manuscript, three dimers were extracted from the unit cell, corresponding to the π-π stacking interaction (dimer 1-2, Figure 2 in main text), and two unique Br…Br / Br…H contacts (dimers 2-3 and 3-4, Figure 2 in main text). The complete energy decomposition using sSAPT0 /jun-cc-pVDZ is give in Tables S1-S3 for dimer 1-2, dimer 2-3 and dimer 3-4, respectively.

Table S1: sSAPT0/jun-cc-pVDZ energy decomposition for dimer 1-2, the π-π stacking interaction, as a function of temperature. The electrostatic (E_{elst}), exchange (E_{exch}), inductive (E_{ind}) and dispersion (E_{disp}). The total energy is also given, E_{IE}^{sSAPT0}. All energies are given in KJ.mol^{-1}.

Temperature /K	E_{elst}	E_{exch}	E_{ind}	E_{disp}	E_{IE}^{sSAPT0}
273	-16.17902211	45.38233539	-2.94333021	-59.27396488	-33.01398181
283	-15.78413961	44.80530302	-2.89705884	-58.82474139	-32.70063682
293	-15.64964792	44.02434433	-2.81818260	-58.50874249	-32.95222868
303	-15.48781490	43.42606161	-2.74388912	-58.18021998	-32.98586239

313	-15.55514747	41.94265461	-2.41712918	-57.79717036	-33.82679240
323	-15.43947264	41.28760973	-2.33558576	-57.42300806	-33.91045673
333	-15.15147261	40.62890226	-2.27528535	-57.14658426	-33.94443995
343	-14.89507049	40.09888829	-2.25001694	-56.69442199	-33.74062113

Table S2: sSAPT0/jun-cc-pVDZ energy decomposition for dimer 2-3, the first Br…Br/Br…H interaction, as a function of temperature. The electrostatic (E_{elst}), exchange (E_{exch}), inductive (E_{ind}) and dispersion (E_{disp}). The total energy is also given, E_{IE}^{sSAPT0} All energies are given in KJ.mol^{-1}.

Temperature /K	E_{elst}	E_{exch}	E_{ind}	E_{disp}	E_{IE}^{sSAPT0}
273	-12.94024417	23.17963726	-2.88224215	-16.85778484	-9.50063391
283	-12.98470084	23.10938772	-2.89938833	-16.83368975	-9.60839119
293	-12.88876523	22.98678464	-2.86690475	-16.81940215	-9.58828750
303	-12.87063838	22.91024784	-2.85500096	-16.80801048	-9.62340198
313	-14.13762637	24.73168880	-3.03121461	-17.55000517	-9.98715736
323	-14.01981239	24.41889095	-3.00371072	-17.47733997	-10.08197213
333	-13.86306614	24.08190860	-2.95693611	-17.36565312	-10.10374677
343	-13.74454978	23.75809006	-2.93813464	-17.24191621	-10.16651057

Table S3: sSAPT0/jun-cc-pVDZ energy decomposition for dimer 3-4, the second Br…Br/Br…H interaction, as a function of temperature. The electrostatic (E_{elst}), exchange (E_{exch}), inductive (E_{ind}) and dispersion (E_{disp}). The total energy is also given, E_{IE}^{sSAPT0} All energies are given in KJ.mol^{-1}.

Temperature /K	E_{elst}	E_{exch}	E_{ind}	E_{disp}	E_{IE}^{sSAPT0}
273	-12.94025043	23.17964092	-2.88211979	-16.85778758	-9.50051687
283	-12.98471361	23.10941667	-2.89944943	-16.83369722	-9.60844359
293	-12.88877111	22.98679573	-2.86688964	-16.81940511	-9.58827013
303	-12.87061847	22.91024779	-2.85502772	-16.80801041	-9.62340882
313	-14.13762279	24.73167049	-3.03137080	-17.55000027	-9.98732336
323	-14.01978386	24.41884256	-3.00363605	-17.47732597	-10.08190332
333	-13.86307033	24.08191297	-2.95699485	-17.36565318	-10.10380538
343	-13.74456654	23.75813126	-2.93815364	-17.24193156	-10.16652048

4. LOBSTER COHP CALCULATIONS

The crystal orbital Hamiltonian population (COHP) offers a means to weight the electronic density of states by the overlap Hamiltonian element. Thus, it offers a measure of the nature and strength of the overlap population. When projected over atomic contributions (pCOHP), this method allows assessment of the covalent character shared between select atom pairs. By integrating the pCOHP up to the Fermi energy (eF), a measure of the covalent bond strength can therefore be obtained. This has been done for all intermolecular Br…Br and Br…H contacts at points immediately before and after the phase transition, Table S4.

Table S4: COHP analysis of Br…Br and Br…H interactions for TBB before and after the phase transition. The integrated pCOHP values are given at the Fermi energy (eF).

T = 303 K			T = 313 K		
Contact	**Distance /Å**	**-ICOHP (eF) /eV**	**Contact**	**Distance /Å**	**-ICOHP (eF) /eV**
Br1…Br6	3.76	0.06491	Br1…Br6	3.73	0.06426
Br1…Br8	3.62	0.08413	Br1…Br8	3.69	0.07375
Br2…Br5	3.76	0.06515	Br2…Br5	3.73	0.06417
Br2…Br7	3.62	0.08388	Br2…Br7	3.69	0.07383
Br3…Br6	3.62	0.08433	Br3…Br6	3.69	0.07424
Br3…Br8	3.76	0.06494	Br3…Br8	3.73	0.06419
Br4…Br5	3.62	0.08408	Br4…Br5	3.69	0.07433
Br4…Br7	3.76	0.06518	Br4…Br7	3.73	0.06411
Br5…Br7	4.48	0.01261	Br5…Br7	4.18	0.02004
Br6…Br8	4.48	0.01265	Br6…Br8	4.18	0.02011
Br1…H22	3.29	0.01305	Br1…H22	3.34	0.02091
Br2…H21	3.29	0.01334	Br2…H21	3.34	0.02090
Br3…H24	3.29	0.01298	Br3…H24	3.34	0.02142
Br4…H23	3.29	0.01327	Br4…H23	3.34	0.02142
Br5…H22	3.14	0.03653	Br5…H22	3.29	0.02267
Br6…H21	3.14	0.03608	Br6…H21	3.29	0.02276
Br7…H24	3.14	0.03637	Br7…H24	3.29	0.02190
Br8…H23	3.14	0.03592	Br8…H23	3.29	0.02199

5. Comparison of Experimental and Theoretical Vibrational Frequencies

To ensure accuracy of the theoretical model used in this work, calculated Raman frequencies were compared to newly collected single crystal Raman spectra, Figure S3, as well as literature Raman data (K. White and Eckhardt, J. Chem. Phys., 1998**, 109**, 208-213) Excellent agreement is found between both experimental spectra and the calculated frequencies, Table S5. Thus, it is apparent that the DFT model employed here represents an accurate description of the Brillouin zone-centre.

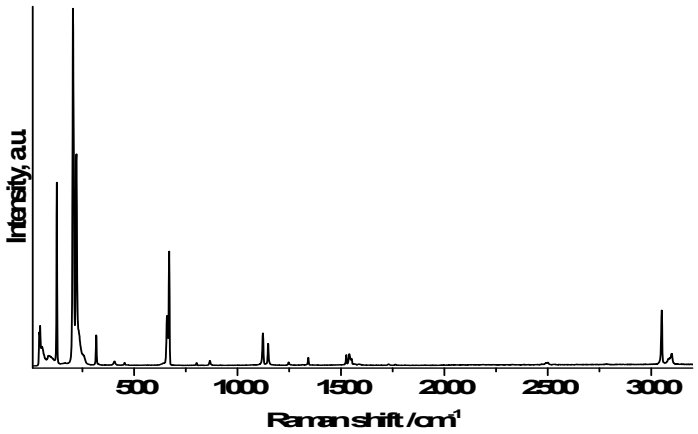

Figure S3: Raman spectrum of a single crystal of *β*-TBB under ambient conditions.

Table S5: Comparison of experimental Raman frequencies with calculated Raman frequencies. Note that only modes calculated as being Raman active are given Here. Literature Raman data taken from [White and Eckhardt, J Chem Phys 109, 1, 1998].

Experimental		Calculated	Assignment
Literature	This work		
--	--	18.13, 19.54, 35.59	TBB external rocking
--	42	42.25	TBB external rocking
--	45.5	43.29, 47.05	TBB external rocking
	54	--	
	87		
125	126.4	123.99, 126.90	Br in-plane wag
203	203.6	196.73, 199.77,	TBB ring rocking
208	209	203.82, 204.21	Ring deformation
220	221	221.21, 221.54	C-Br Stretch
--	234	--	
--	256	--	
317	317	313.75, 314.21	TBB ring rocking
--	403	--	
453	454	455.70, 457.32	TBB ring twisting
657	659	653.00. 655.97,	Ring deformation
667	669	659.19	Ring deformation
--	--	777.55	Ring deformation
800	802	790.19	Ring deformation
866	866, 868	849.45, 850.52	H wag, ring deformation

In contrast to the present work, earlier reports of the Raman spectra of TBB under ambient conditions do not discuss the presence of a Raman active band at *ca* 100 cm^{-1}, or at *ca* 400 cm^{-1}. Indeed, calculations based on the harmonic approximation also suggests that these bands should not be present. The presence of these bands in the spectrum presented in this work can therefore be attributed to overtone modes.

Given the excellent agreement between experimental and calculated Raman spectra, the vibrational frequencies across all temperature points were calculated, Table S6.

Table S6: Calculated zone-centre vibrational frequencies for TBB at a variety of temperatures. All calculations based on experimentally determined crystal structures at the corresponding temperature. The corresponding symmetry species is given for each frequency (point group C2h)

	273 K		283 K		293 K		303 K	
No.	**Frequency**	**Symmetry**	**Frequency**	**Symmetry**	**Frequency**	**Symmetry**	**Frequency**	**Symmetry**
1	-0.030061	A_u	-0.030088	A_u	-0.030239	A_u	-0.030439	A_u
2	-0.024501	B_u	-0.024590	B_u	-0.024631	B_u	-0.024563	B_u
3	-0.017590	B_u	-0.017609	B_u	-0.017627	B_u	-0.017616	B_u
4	18.133372	B_g	17.549431	B_g	17.682077	B_g	18.615016	B_g
5	19.540091	A_g	18.787559	A_g	18.540616	A_g	18.959618	A_g
6	30.522831	A_u	29.581547	A_u	30.117160	A_u	32.116470	A_u
7	35.586655	A_g	35.567965	A_g	35.425034	A_g	35.745394	A_g
8	42.250685	B_g	42.024790	B_g	41.828934	B_g	41.520602	A_g
9	43.290928	A_g	42.587388	A_g	41.864921	A_g	41.708368	B_g
10	44.647460	A_u	44.364859	A_u	42.946964	A_u	44.064299	A_u
11	47.055407	B_g	46.588669	B_g	45.589936	B_g	45.164879	B_g
12	52.229905	A_u	51.803833	A_u	51.375750	A_u	51.390016	A_u
13	52.624787	B_u	52.177712	B_u	52.382373	B_u	52.920084	B_u
14	61.116719	B_u	59.810296	B_u	59.146497	B_u	58.838457	B_u
15	110.518449	A_u	109.697737	A_u	109.602561	A_u	110.556675	A_u
16	112.444720	B_u	111.906967	B_u	111.755910	B_u	112.359933	B_u
17	123.987770	B_g	123.882690	B_g	123.773765	B_g	123.699191	B_g
18	126.902117	A_g	126.753075	A_g	126.604584	A_g	126.487730	A_g
19	131.839536	A_u	131.670793	A_u	131.556582	A_u	131.664939	A_u
20	134.351293	B_u	134.154707	B_u	134.292480	B_u	134.706092	B_u
21	143.060087	B_u	142.746219	B_u	142.534961	B_u	142.708450	B_u
22	147.111567	A_u	146.496840	A_u	146.271072	A_u	146.528838	A_u
23	196.741936	B_g	196.528470	B_g	196.595228	B_g	197.100594	B_g
24	199.771987	A_g	199.530719	A_g	199.704210	A_g	200.220908	A_g
25	203.818325	A_g	203.719280	A_g	203.694378	A_g	203.860728	A_g
26	204.211053	B_g	204.061438	B_g	204.151191	B_g	204.377839	B_g
27	221.207521	B_g	221.164006	B_g	221.147965	B_g	221.137400	B_g
28	221.540814	A_g	221.527723	A_g	221.506440	A_g	221.504831	A_g
29	313.751440	A_g	313.139385	A_g	313.049180	A_g	313.707374	A_g
30	314.212827	B_g	313.594756	B_g	313.498929	B_g	314.154112	B_g
31	384.334707	B_u	383.699459	B_u	383.476684	B_u	384.002929	B_u
32	384.711855	A_u	384.503051	A_u	384.192995	A_u	384.906856	A_u
33	425.171334	A_u	425.157787	A_u	425.379137	A_u	425.793863	B_u
34	425.300307	B_u	425.304575	B_u	425.434771	B_u	425.856678	A_u
35	455.704660	B_g	454.983867	B_g	454.405760	B_g	455.174505	B_g

36	457.315064	A_g	456.600054	A_g	456.009141	A_g	456.768681	A_g
37	519.170984	A_u	519.307684	A_u	519.294246	A_u	519.246290	A_u
38	519.995396	B_u	519.970411	B_u	519.818587	B_u	519.775977	B_u
39	566.545075	A_u	566.252942	A_u	566.246034	A_u	566.665379	B_u
40	566.559235	B_u	566.269081	B_u	566.255631	B_u	566.667705	A_u
41	652.995796	A_g	652.954254	A_g	652.749645	A_g	652.673584	A_g
42	655.973380	B_g	655.982833	B_g	655.737237	B_g	655.533155	B_g
43	657.884112	A_g	657.751755	A_g	657.771686	A_g	658.038321	A_g
44	659.194513	B_g	659.046483	B_g	659.106994	B_g	659.506721	B_g
45	777.543635	A_g	777.330305	A_g	777.849685	A_g	778.599982	A_g
46	790.055395	B_g	789.821864	B_g	790.292859	B_g	790.985133	B_g
47	849.459598	B_g	849.594630	B_g	849.794688	B_g	850.026898	B_g
48	850.521976	A_g	850.648705	A_g	850.832917	A_g	851.050515	A_g
49	869.141439	A_u	869.273617	A_u	869.446382	A_u	869.616949	A_u
50	869.258037	B_u	869.475583	B_u	869.610432	B_u	869.688571	B_u
51	995.981734	A_u	995.850289	A_u	996.179092	A_u	996.670046	A_u
52	997.195733	B_u	996.999644	B_u	997.227534	B_u	997.590382	B_u
53	1098.869937	A_g	1098.758571	A_g	1098.944810	A_g	1099.197427	A_g
54	1099.965905	B_g	1099.876960	B_g	1100.060305	B_g	1100.311798	B_g
55	1105.807071	A_u	1105.501864	A_u	1105.523809	A_u	1105.602088	A_u
56	1106.197003	B_u	1105.933828	B_u	1105.797084	B_u	1105.763894	B_u
57	1247.037052	A_g	1246.792624	A_g	1246.480314	A_g	1246.260687	A_g
58	1250.276655	B_g	1250.010230	B_g	1249.679293	B_g	1249.458586	B_g
59	1275.821954	A_u	1275.632677	A_u	1275.160879	A_u	1275.426377	A_u
60	1275.910091	B_u	1275.782582	B_u	1275.364795	B_u	1275.647557	B_u
61	1281.613611	A_u	1281.273048	A_u	1280.943330	A_u	1280.683352	A_u
62	1281.984530	B_u	1281.605977	B_u	1281.275747	B_u	1281.043881	B_u
63	1412.638187	A_u	1412.468761	A_u	1412.389341	A_u	1412.398788	A_u
64	1413.971087	B_u	1413.726493	B_u	1413.641790	B_u	1413.580532	B_u
65	1492.534216	A_g	1492.101245	A_g	1491.786689	A_g	1492.122614	A_g
66	1493.103565	B_g	1492.668481	B_g	1492.358839	B_g	1492.677373	B_g
67	1514.665479	A_g	1514.546125	A_g	1514.354706	A_g	1514.187741	A_g
68	1526.185947	B_g	1526.054183	B_g	1525.833163	B_g	1525.651779	B_g
69	3106.761987	A_u	3106.481733	A_u	3106.034353	A_u	105.611022	A_u
70	3107.058810	B_u	3106.779221	B_u	3106.383671	B_u	105.909621	B_u
71	3108.330122	A_g	3108.016382	A_g	3107.583594	A_g	107.165835	A_g
72	3109.135823	B_g	3108.810925	B_g	3108.364098	B_g	3107.932600	B_g

	313 K		323 K		333 K		343 K	
No.	**Frequency**	**Symmetry**	**Frequency**	**Symmetry**	**Frequency**	**Symmetry**	**Frequency**	**Symmetry**
1	-0.029517	B_u	-0.029036	B_u	-0.029736	B_u	-0.030407	B_u
2	-0.017572	A_u	-0.017581	A_u	-0.017546	A_u	-0.017521	A_u
3	0.060192	B_u	0.071406	B_u	0.079043	B_u	0.076759	B_u
4	16.804768	A_g	15.936078	A_g	15.230891	A_g	15.249326	A_g
5	21.024886	B_g	21.483357	B_g	21.714037	B_g	22.137112	B_g
6	32.667883	A_u	32.573506	A_u	31.554755	A_u	30.905675	A_u
7	35.778551	B_g	34.244233	B_g	33.459799	B_g	32.989364	B_g
8	36.718012	A_g	36.137521	A_g	35.356180	A_g	34.837655	A_g
9	38.159122	A_g	38.263060	A_g	38.082080	A_g	38.009648	A_g
10	43.296761	B_g	42.849476	B_g	42.458830	B_g	42.284857	B_g
11	43.782009	B_u	45.120047	B_u	44.576709	B_u	44.380616	B_u
12	45.971322	A_u	45.560018	A_u	45.166900	A_u	44.838301	A_u
13	51.227139	A_u	50.680247	A_u	50.190193	A_u	49.826384	A_u
14	51.740520	B_u	51.627229	B_u	51.301662	B_u	51.124024	B_u
15	115.409492	A_u	115.026259	A_u	113.940135	A_u	113.332903	A_u
16	116.449751	B_u	115.702923	B_u	114.725715	B_u	114.216710	B_u
17	123.425832	B_g	123.751438	B_g	123.524938	B_g	123.419254	B_g
18	125.793572	A_g	125.653941	A_g	125.487762	A_g	125.449889	A_g
19	132.789565	A_u	132.792544	A_u	132.638123	A_u	132.538750	A_u
20	134.172739	B_u	133.896209	B_u	133.673878	B_u	133.550543	B_u
21	142.491397	A_u	142.275795	A_u	141.836837	A_u	141.568781	A_u
22	142.671192	B_u	142.718733	B_u	142.477562	B_u	142.333020	B_u
23	199.666000	B_g	198.506942	B_g	196.954715	B_g	195.949511	B_g
24	201.425294	A_g	200.622958	A_g	199.305732	A_g	198.340382	A_g
25	204.445801	A_g	204.198375	A_g	203.853903	A_g	203.727096	A_g
26	204.743503	B_g	204.704575	B_g	204.525151	B_g	204.455713	B_g
27	220.929892	B_g	220.857126	B_g	220.803868	B_g	220.785808	B_g
28	221.563210	A_g	221.522167	A_g	221.429014	A_g	221.400329	A_g
29	317.756213	A_g	318.245361	A_g	318.672717	A_g	319.184992	A_g
30	318.009124	B_g	318.529669	B_g	319.021596	B_g	319.556833	B_g
31	382.679206	B_u	383.362332	B_u	383.261008	B_u	383.014576	B_u
32	384.329723	A_u	384.369688	A_u	384.190871	A_u	383.912939	A_u
33	428.715375	B_u	428.619843	B_u	428.357503	B_u	428.205784	B_u
34	429.127105	A_u	429.026746	A_u	428.728004	A_u	428.564974	A_u

35	453.401692	B_g	453.639196	B_g	453.714249	B_g	453.621611	B_g
36	454.846683	A_g	455.187082	A_g	455.260899	A_g	455.157165	A_g
37	519.291676	B_u	519.165449	A_u	518.936216	A_u	518.796573	A_u
38	519.332909	A_u	519.312128	B_u	519.159519	B_u	519.068870	B_u
39	568.612128	B_u	568.908115	B_u	569.179934	B_u	569.445811	B_u
40	568.677467	A_u	568.965679	A_u	569.237817	A_u	569.513548	A_u
41	651.883284	A_g	651.700427	A_g	651.158800	A_g	650.725259	A_g
42	654.835360	B_g	654.649719	B_g	654.108144	B_g	653.674469	B_g
43	660.057786	A_g	660.168412	A_g	660.203151	A_g	660.310304	A_g
44	661.464397	B_g	661.568034	B_g	661.574017	B_g	661.662128	B_g
45	778.441868	A_g	778.253916	A_g	778.058792	A_g	777.967948	A_g
46	790.440411	B_g	790.284969	B_g	790.048284	B_g	789.932935	B_g
47	851.680843	B_g	851.612710	B_g	851.434138	B_g	851.322207	B_g
48	852.400119	A_g	852.297731	A_g	852.091972	A_g	851.956979	A_g
49	871.023257	A_u	870.955618	A_u	870.788271	A_u	870.670928	A_u
50	871.322784	B_u	871.316001	B_u	871.238345	B_u	871.141889	B_u
51	996.997810	A_u	996.846021	A_u	996.619317	A_u	996.485687	A_u
52	997.658647	B_u	997.418211	B_u	997.105655	B_u	996.894076	B_u
53	1098.466422	A_g	1098.252008	A_g	1097.902330	A_g	1097.738963	A_g
54	1099.578734	B_g	1099.127358	B_g	1098.841404	B_g	1098.694245	B_g
55	1102.558188	A_u	1102.328416	A_u	1102.139942	A_u	1102.002878	A_u
56	1104.174570	B_u	1104.037634	B_u	1103.916463	B_u	1103.851929	B_u
57	1243.387747	A_g	1243.304338	A_g	1243.212881	A_g	1243.135349	A_g
58	1246.524769	B_g	1246.419709	B_g	1246.294374	B_g	1246.189624	B_g
59	1275.953037	A_u	1276.039196	A_u	1275.961028	A_u	1275.946107	A_u
60	1276.969349	B_u	1277.040624	B_u	1277.003208	B_u	1277.053365	B_u
61	1277.887328	A_u	1277.833129	A_u	1277.619081	A_u	1277.458670	A_u
62	1278.701965	B_u	1278.637711	B_u	1278.389174	B_u	1278.169378	B_u
63	1410.902781	A_u	1410.754812	A_u	1410.583745	A_u	1410.489430	A_u
64	1413.269139	B_u	1413.086776	B_u	1412.905413	B_u	1412.821895	B_u
65	1491.335828	A_g	1491.431204	A_g	1491.368989	A_g	1491.336790	A_g
66	1491.681437	B_g	1491.826781	B_g	1491.738781	B_g	1491.693942	B_g
67	1512.987625	A_g	1512.896711	A_g	1512.709186	A_g	1512.615246	A_g
68	1524.182781	B_g	1524.067906	B_g	1523.827807	B_g	1523.711420	B_g
69	3103.099881	A_u	3103.014470	A_u	3102.935091	A_u	3102.919093	A_u
70	3103.420390	B_u	3103.332830	B_u	3103.249753	B_u	3103.236360	B_u
71	3104.449916	A_g	3104.368725	A_g	3104.285966	A_g	3104.263503	A_g

72	3105.138397	B_g	3105.040722	B_g	3104.940348	B_g	3104.907742	B_g

The phase transition is met with marked shift in the low frequency vibrational structure. However, there is little change associated with the eigenvectors in each polymorph, with 8 of the 11 low frequency modes mapping directly from one phase to other (albeit at notably different frequencies), Table S7.

Table S7: Mapping of low frequency vibrational modes from *β*-TBB (303 K) to *γ*-TBB (313 K). Where direct mapping does not occur, a cell is marked '- -'. The symmetry species (point group C2h) are listed.

303 K /cm^{-1}	Symmetry 303 K	313 K /cm^{-1}	Symmetry 313 K
18.62	Ag	16.80	Ag
18.96	Bg	21.02	Bg
32.12	Au	32.67	Au
35.75	Ag	--	--
41.52	Ag	36.72	Ag
41.71	Bg	35.78	Bg
44.06	Au	--	--
--	--	38.16	Ag
--	--	43.30	Bg
45.16	Bg	--	--
51.39	Au	45.97	Au
--	--	51.23	Au
52.92	Bu	51.74	Bu
58.85	Bu	43.78	Bu

7. TEMPERATURE VARIATION OF VIBRATIONAL FREQUENCIES IN *β*- AND *γ*-TBB

The vibrational response to heating of *β*-TBB is complex, Figure S4. All modes are seen to initially soften between 273 K and 283 K, in agreement with discontinuities in pairwise interaction energies. Very many of these modes, however, continue to soften only until 293 K, before suddenly hardening by 303 K. Only three modes 9, 11 and 14, are seen to soften monotonically towards the phase transition.

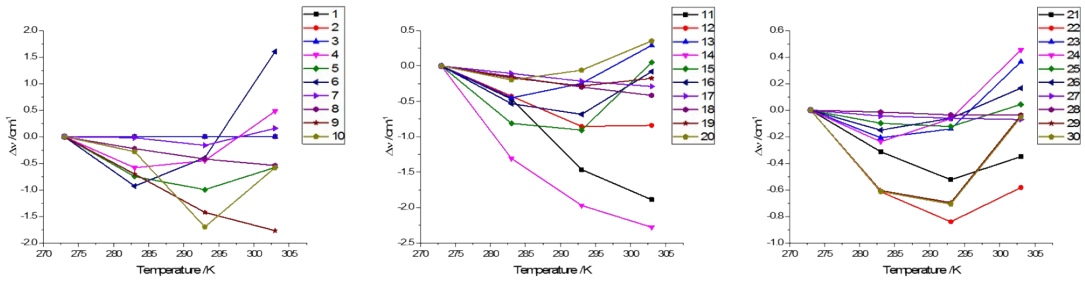

Figure S4: Variation in low frequency *β*-TBB zone-centre vibrational frequencies as a function of temperature. Modes are labelled according to mode number according to Table S6.

On further heating beyond the phase transition, the vibrational frequencies display a more typical response to thermal expansion. That is, nearly all modes are found to soften with increasing temperature, Figures S5.

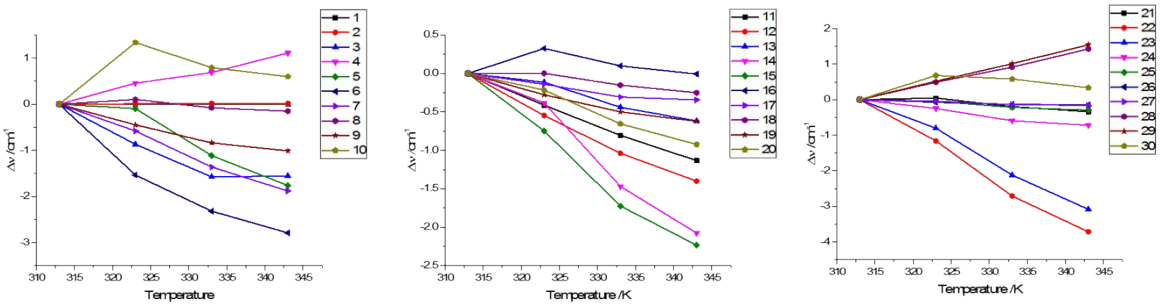

Figure S5: Variation in low frequency *γ*-TBB zone-centre vibrational frequencies as a function of temperature. Modes are labelled according to mode number according to Table S6.

8. Eigenvectors of Notable Normal Modes

While the majority of low frequency modes are seen to first soften, before hardening at the phase transition temperature, Figure S4, this effect is largest for the Au mode [32.12 cm^{-1} T=303 K] that corresponds to translation of π-stacked columns, Figure S6

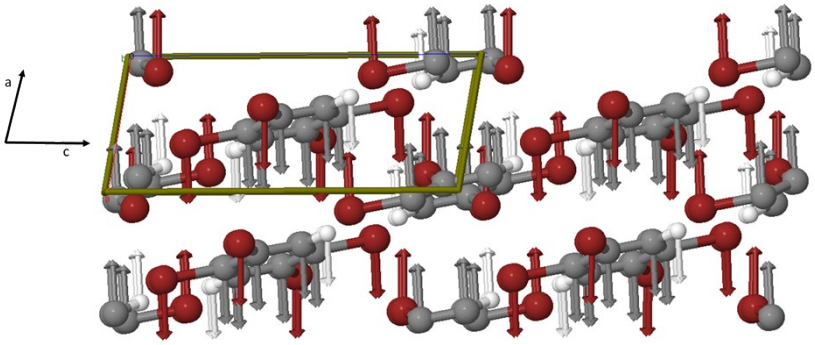

Fig S6: The normal mode in *β*-TBB that displays largest hardening towards the phase transition. Eigenvectors are shown with arrows.

Only three vibrational modes are found to monotonically soften towards the phase transition on heating, Figure S4. These correspond to two rocking modes, and a translation, Figure S7.

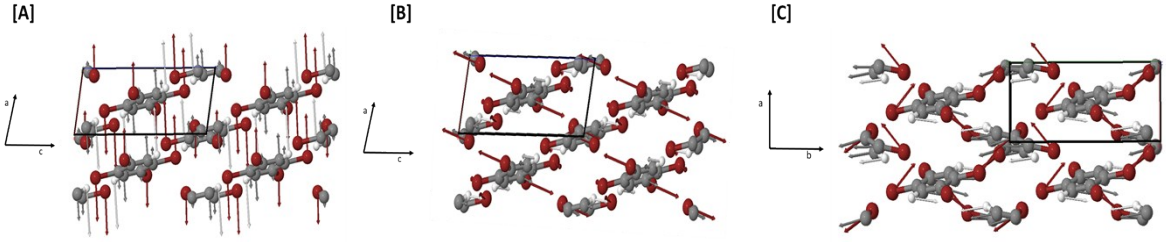

Figure S7: (A) B_g soft mode 43.29 cm^{-1} at T=273 K, (B) B_g soft mode 47.05 cm^{-1} at T=273 K, and (C) B_u soft mode at 61.12 cm^{-1} at T=273 K.

The soft mode with large translational component along the crystallographic *b*-axis, Figure S7c, has a net displacement vector associated with it, Figure S8.

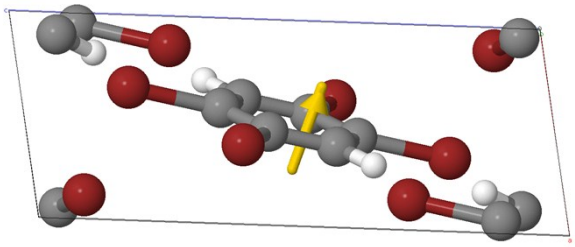

Figure S8: Net displacement direction yellow arrow of the Bu soft mode in the *β*-TBB lattice.

Across the phase transition, only three modes are found not to be conserved, Figure S9. While the symmetry of these modes is obviously conserved, the main polarisation of their eigenvectors shifts drastically, and is likely responsible for immense build-up of stress at domain interfaces.

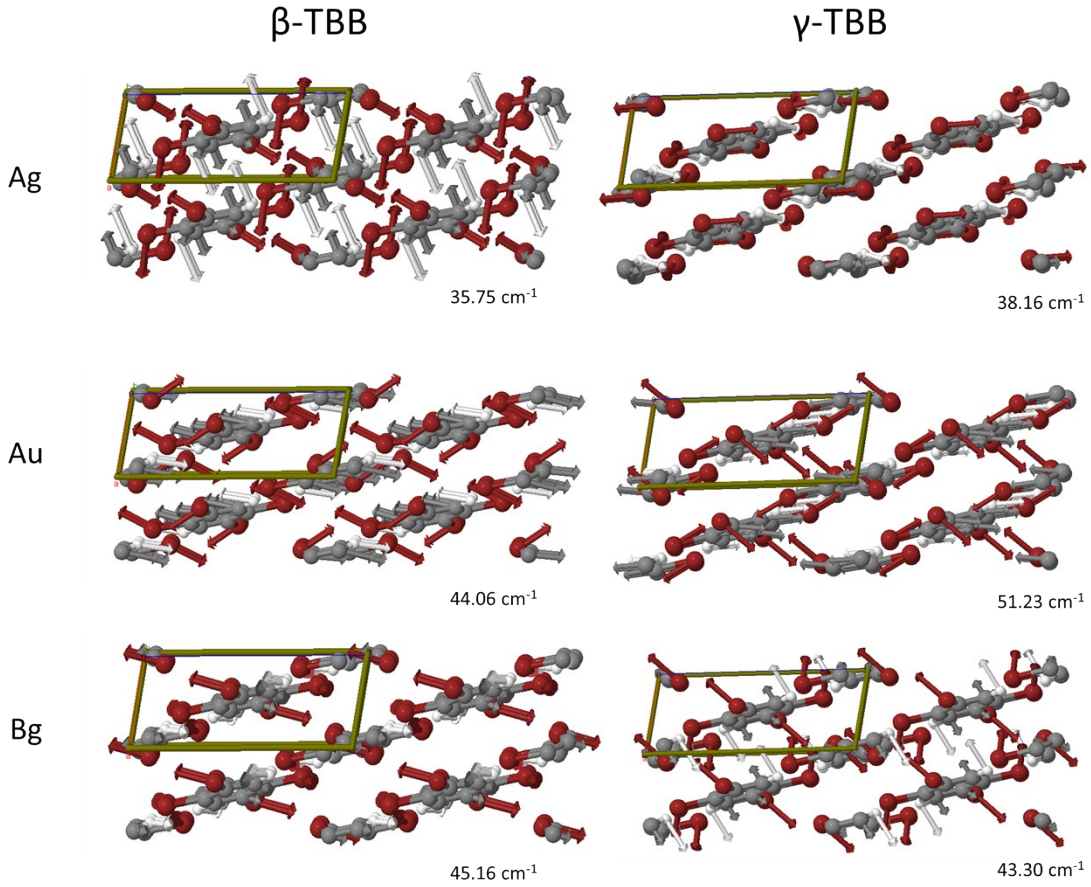

Figure S9: Eigenvectors of the non-mapped normal coordinates across the TBB phase transition. Mode symmetry and associated vibrational frequency are shown. Arrows indicate direction of atomic displacement.